A Method for Static and Dynamic Load Analysis of Standard and Modified Spur Gears*

Romualdas Kasuba†

Many advanced technology applications have a general requirement that the power to transmission weight be increased. Engineers, as a result of those requirements, attempt to design gear systems to maximum load capacity. For this purpose the ability to accurately calculate the dynamic loads becomes essential for advanced transmission design. Most of the previously proposed methods (refs. 1 to 8) are limited to the normal contact ratio (NCR) gearing and are based on a number of simplifications, which can be generalized as follows:

(a) Gear-tooth errors have negligible or no effect on mesh stiffness. This implies that, for a given load, a gear with errors will have equal mesh stiffness as the same gear without errors.

(b) Contact is assumed to occur only on the line of action.

(c) The contact ratio (CR) and/or mesh stiffness are not affected by transmitted load or premature or delayed engagement.

(d) Dynamic simulations use uninterrupted periodic rectangular stiffness functions and error displacement strips.

The high-contact-ratio (HCR) gearing is also considered for many applications. However, the number of available methods for analyzing the HCR gearing is very limited. A parametric static analysis of HCR gearing was published by Staph (ref. 9) in 1975. A Richardson-type cam model was extended by Cornell and Westervelt in 1977 (ref. 10). In 1980 Kasuba and Evans presented an extended digitized model for determining the gear-mesh stiffness and dynamic loads for any operational contact ratio (ref. 11). This method removes the previously listed simplifications mentioned in the previous paragraph. In this case the variable gear-mesh stiffness is determined by solving the statically indeterminate problems of multipair contact gear-tooth error effects on contacting point locations and gear-tooth and gear-hub deflections. Importantly, this method does not rely on the commonly used assumption that a gear pair with errors has the same gear-mesh stiffness as an identical pair without errors. Such an assumption would be completely unacceptable in analysis of HCR gearing. Gear-tooth errors can cause interruptions of gear-mesh stiffness and, thus, affect the dynamic loads in gearing. Identical gear-tooth errors in the NCR and HCR spur gearing affect the mesh stiffness and dynamic loads to different degrees. This paper discusses the mesh stiffness and dynamic load characteristics for several cases of the NCR and HCR gearing. The considered contact ratios were grouped in the general range of 1.7, 2.0, and 2.3.

In this study the HCR gearing is defined by contact ratios equal to or greater than 2.0. The HCR gearing in this study is represented by a group of small pressure angle, fine pitch, and long addendum gearing.

Nomenclature

BGM	backlash
C	center distance
C_B	bearing damping
C_S	shaft damping
CR	loaded contact ratio
CR_T	theoretical contact ratio
DF	dynamic load factor

*This paper is based in part on work supported by NASA Lewis Research Center and the U.S. Army Aviation Research and Technology Laboratories under NASA contract NAS3-18547.

†Fenn College of Engineering, Cleveland State University.

E	Young's modulus
F	gear face width
F_H	hub face width
G	torsional modulus
GP	gear-tooth pair
HSF	hub torsional stiffness factor
J	mass moment of inertia
J_G	$\frac{1}{2}\, M_G/(\mathrm{RBC})^2$
K	shaft stiffness
KG	gear-mesh stiffness, N/m
KP	gear pair stiffness, N/m
M	mass
P_H	Hertz stress
PE	profile error
PM	profile modification
PSITP	static angular position
PV	$P_H \times C$, N/m sec
Q	static GP load, normal
Q_t	total mesh static load, normal
QD	dynamic GP load, normal
QD_t	total mesh dynamic load, normal
RA	roll angle
RABOT	RA at bottom of involute
RAPP	RA at pitch point
RATIP	RA at tip of involute
RBC	radius of base circle
RCCP	radius of curvature
RCP	radius to contacting point
RH_f	hub fixity radius
RRC	radius of root circle
TR	transmission ratio
V	sliding velocity
μ	Poisson's ratio
δ	deflection
ξ	critical damping ratio, gear mesh
ξ_S	critical damping ratio, shafts
ψ	dynamic displacement, rad
$\dot{\psi}$	dynamic velocity, rad/sec

Subscripts:

D	driving element
G	gear
HRC	high contact ratio gearing
i	mesh arc position
k	k^{th} gear-tooth pair
L	load element
NCR	normal contact ratio gearing

S	shafting
1	gear 1
2	gear 2
$'$	instantaneous

Definition of Spur Gear Tooth Profiles and Coordinates

The variable gear-mesh stiffness is a function of load, errors, position of contact, gear and hub geometry, and respective deflections. For this purpose the actual gear-tooth profiles must be used.

By employing the involute chart approach (figs. 1 to 3), a number of gear-tooth profiles can be

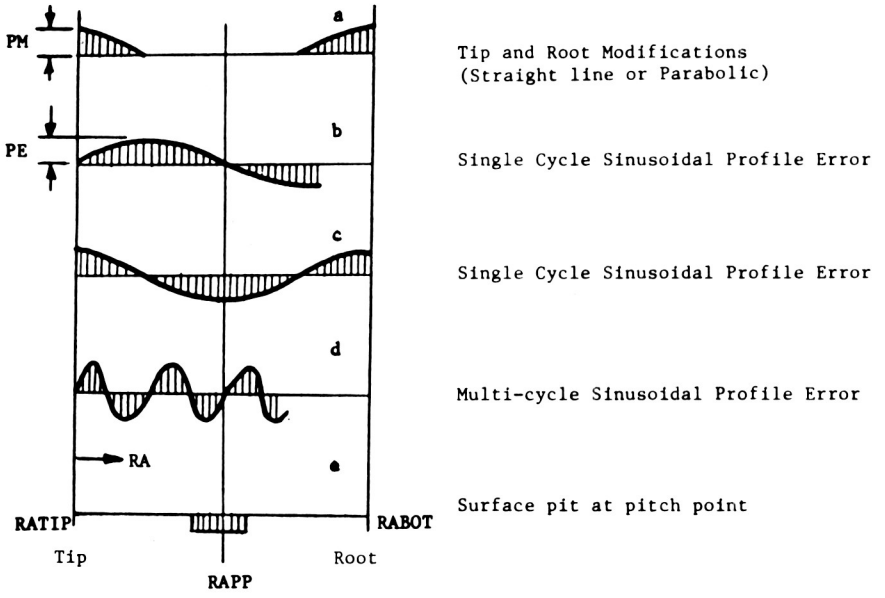

Figure 1. - Sample simulated gear tooth profile charts.

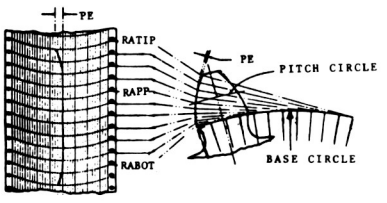

Figure 2. - Involute chart - profile relationship.

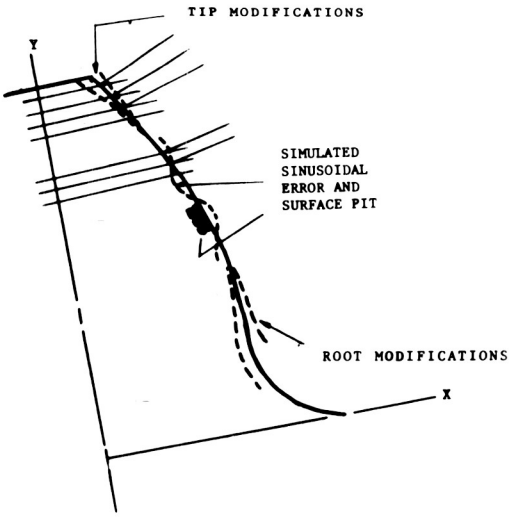

Figure 3. - Gear tooth profiles.

defined. The profile modifications (PM) and profile errors (PE) can be expressed as

$$\Delta M = \delta P(\mathrm{RA}) \tag{1}$$

where

ΔM deviation from the line of action
RA roll angle limited to active profile
δP profile variation (error or amount of modification) as a function of RA

A true involute profile is defined by

$$\Delta M = \delta P(\mathrm{RA}) = 0$$

(straight line in involute chart).

For example, the simulated profile chart can accommodate the parabolic and straight-line modifications of the tip and root zones (fig. 1(a)). The profile errors can be approximated by sinusoidal representation. By varying the number of cycles and phase angle, the sinusoidal profile errors (figs. 1(b) to (d)) could describe a large number of practical and theoretical cases. A simulated surface pitting damage is shown in figure 1(e). The defined surface faults and their respective involute charts are then numerically transferred to the previously digitized true involute profile. This is accomplished by subtracting or adding the specified amounts of material perpendicularly to the true involute profile, as shown in figures 2 and 3.

The digitized profile points and the subsequent deflections were analyzed in a rotating gear pair coordinate system. The position of contacting points, number of contacting tooth pairs, operational contact ratio, and variable gear-mesh stiffness were established by iterative procedures under fully loaded and deflected conditions. Five gear-tooth pairs are analyzed in search of potential contacting points. Figure 4 illustrates the general gear and gear-tooth coordinate system. For establishing the points of contact, load transfers, and deflections within the mesh arc, three coordinate systems are used:

(1) U, V—Fixed global coordinate system for the pinion and gear-tooth profiles, gears 1 and 2, respectively. The U, V coordinate system is used to determine the number of contacting pairs and position of contacting points.

(2) X, Y—Local coordinate system fixed at the root of individual teeth for the pinion and gear, respectively. The Y-axes coincide with the tooth centerlines. The X, Y coordinate system is used in digitizing the profiles and for determining the appropriate deflections of the teeth.

(3) W, Z—Intermediate coordinate system rotating with the pinion and gear, respectively. The origins of the W, Z coordinate systems for each gear are at the respective gear centers. The Z-axes coincide with the tooth centerlines.

The transformations between the coordinate systems for each considered gear pair ($k = 1, n$) are

$$\begin{aligned}
&\mathrm{W1} = \mathrm{X1};\ \mathrm{W2} = \mathrm{X2}(2)\\
&\mathrm{Z1} = \mathrm{Y1} + \mathrm{RR01};\ \mathrm{Z2} = \mathrm{Y2} + \mathrm{RR02}\\
&\mathrm{U1} = \mathrm{W1}\ \sin\ \mathrm{PSI1TP}(k) + \mathrm{Z1}\ \cos\ \mathrm{PSI1TP}(k)\\
&\mathrm{V1} = -\mathrm{W1}\ \cos\ \mathrm{PSI1TP}(k) + \mathrm{Z1}\ \sin\ \mathrm{PSI1TP}(k)\\
&\mathrm{U2} = -\mathrm{W2}\ \cos\ (\mathrm{PSI2TP}(k) - 1.5\ \pi) + \mathrm{Z2}\ \sin\ \mathrm{PSI2TP}(k) - 1.5\ \pi)\\
&\mathrm{V2} = \mathrm{C} - [\mathrm{W2}\ \sin\ (\mathrm{PSI2TP}(k) - 1.5\ \pi) + \mathrm{Z2}\ \cos\ (\mathrm{PSI2TP}(k) - 1.5\ \pi)]
\end{aligned} \tag{2}$$

Determination of Gear Tooth Deflections and Gear Mesh Stiffness

The digitized profile points describe each gear tooth in space and include the profile errors and modifications. In the iteration process the digitized points also incorporate the appropriate

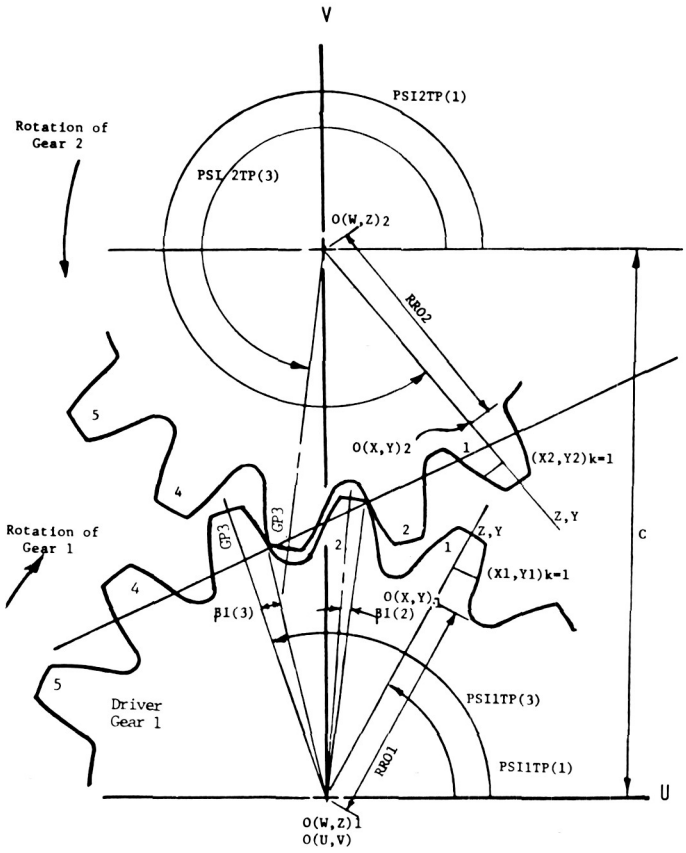

Figure 4. - Gear tooth coordinate system.

deformations to simulate the noninvolute action caused by gear-tooth deflections.

The contacting points on the gear teeth and the number of contacting gear-tooth pairs are determined by using a three-step process. First, the gears are preloaded by a unit load and rotated by incrementing the PSI1TP(k) and PSI2TP(k) angles and examining the potential contact between the calculated (U1(k), V2(k)) profile points for five gear-tooth pairs. The beginning and the end of the meshing arc are established by tracking gear pair 3 (GP3) through its complete meshing arc. After the limiting points of mesh arc are determined, the mesh arc is divided into 50 segments. Next, the gears are fully loaded for further analysis. The actual load sharing and deflections are calculated for 50 arc segments by tracking the movement of fully loaded gears through the established mesh arc.

The gear-tooth pair deflection $(k)_i$ can be expressed in the following form:

$$\delta(k)_i = \delta_1(k)_i + \delta_2(k)_i + \delta_H(k)_i \tag{3}$$

where

$\delta_1(k)_i$ deflection of the k^{th} tooth of gear 1 at mesh arc position i

$\delta_2(k)_i$ deflection of the k^{th} tooth of gear 2 at mesh arc position i

$\delta_H(k)_i$ localized Hertz deformation at the point of contact

For the contacting pairs the gear-tooth deflections $\delta_1(k)_i$ and $\delta_2(k)_i$ incorporate a number of constituent deflections:

$$\delta_1(k)_i = \delta_{M1}(k)_i + \delta_{N1}(k)_i + \delta_{S1}(k)_i + \delta_{B1}(k)_i + \delta_{R1}(k)_i \tag{4}$$

and similarly for gear 2. In equation (4)

δ_M gear-tooth deflection due to bending

δ_N gear-tooth deflection due to normal force

δ_S gear-tooth deflection due to shear force

δ_B gear-tooth deflection due to deformation of surrounding hub area (rocking action)

δ_R gear-tooth deflection due to gross torsion of the rim or hub

The general gear-tooth deflection model is shown in figure 5. Numerical integration of digitized gear-tooth slices was used to obtain the δ_M, δ_N, and δ_S deflections. The circumferential deformation of the gear hub and deformation of the adjacent part of the gear body were reflected to the contacting point as (δ_R) and (δ_B) deflections, respectively.

The methods for calculating the δ_B and the localized Hertzian deflection δ_H are amply described in references 13 to 15. The δ_R deflections cannot be easily defined. Following the method of reference 14, these deflections can be approximated by employing equation (5). For gear 1

$$\delta_{R1}(k)_i = \frac{Q(k)_i(\mathrm{RCP1}(k)_i)^2 \cos \alpha_{B1}}{4 \times \mathrm{G1(FH1)}} \left[\left(\frac{1}{\mathrm{RH1}_f} \right)^2 - \left(\frac{1}{\mathrm{RH1}_o} \right)^2 \right] \tag{5}$$

where

$Q(k)_i$ load along instantaneous line of action at contact point, k^{th} pair

RCPI(k) radius to the contacting point (gear 1) k^{th} pair (fig. 6)

FH1 hub face (gear 1)

$\mathrm{RH1}_o$ outside hub/rim radius (gear 1)

$\mathrm{RH1}_f$ effective radius of circumferential hub fixity (gear 1)

G1 torsional modulus of elasticity (gear 1)

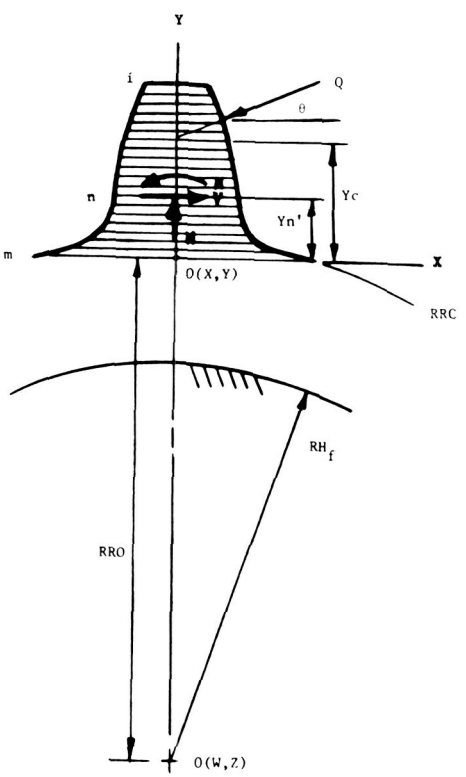

Figure 5. - Gear tooth deflection model.

A similar expression can be given for gear 2, $\delta_{R2}(k)_i$.

The gear-tooth deflections can be considered as equivalent positive profile errors for the pinion and gears causing premature engagement and delayed disengagement (ref. 12). The presence of positive manufactured profile errors (material addition) will increase the total equivalent positive error at the point of contact. Thus, the point of contact will occur farther away from the theoretical line of contact and cause an earlier engagement. The negative profile errors or material removal at the tips will reduce the equivalent positive errors.

In the third step the $\delta_1(k)_i$ and $\delta_2(k)_i$ and apportioned $\delta_H(k)_i$ deflections were returned to equations (2) and added perpendicularly to the respective digitized profiles in order to simulate the above gear behavior. Now, the iterative search and calculation process is repeated under the "loaded and deflected" conditions. In this step the contacting points and the mesh are determined under full load. These events are illustrated in figure 6, where the limiting points of meshing arc occur at points A′ and B′, as compared with the theoretical true involute mesh arc A–B under no load. As a result, the contact arc, and therefore the contact ratio of the gears, is increased. In the same procedural step the final number of pairs in contact, locations of contacting points, gear-tooth deflections, load shearing, stiffness, etc., are computed as the loaded gear-tooth pairs move through the mesh arc A′–B′.

If the geometrical variations in surfaces do not permit contact in steps 1 and 2, then the noncontacting gear teeth are still subjected to δ_R deflections. For example, if GP1 and GP3 are in contact, then for GP2

$$\delta_1(2)_i = \delta_{R1}(2)_i \quad \text{and} \quad \delta_2(2)_i = \delta_{R2}(2)_i \tag{6}$$

These deflections are due to torque transmission at GP1 and GP3 and the resulting circumferential hub deformations at GP2. If the $\delta_1(2)_i$ and $\delta_2(2)_i$ deflections are sufficiently large to overcome the geometrical gap (errors) between the approaching teeth profiles of gears 1 and 2 at the

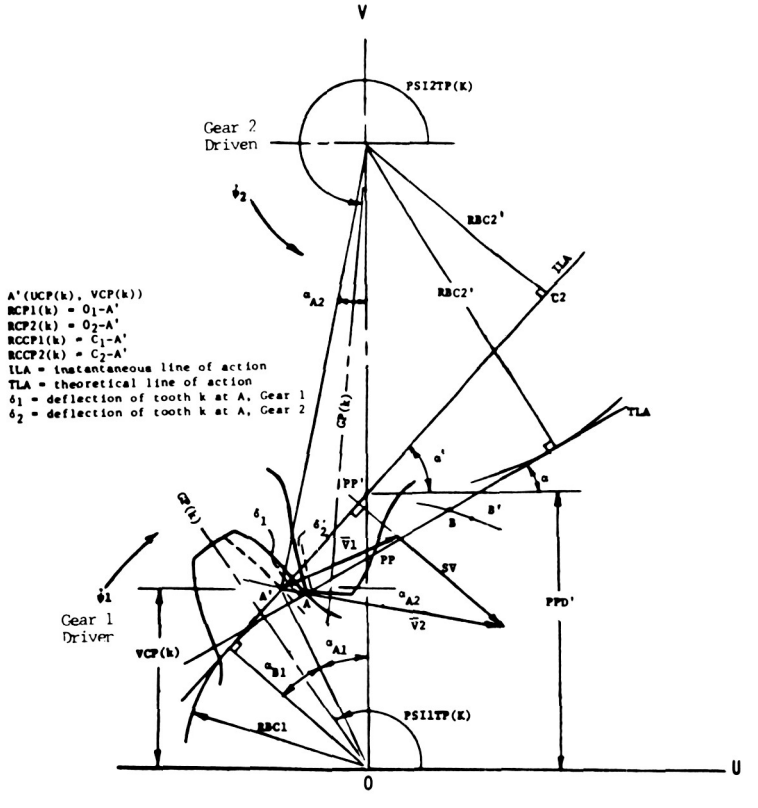

Figure 6. - Instantaneous contact point for incoming gear tooth pair.

angular position i, then the contact will be established for GP2. In this case the final load sharing and deflections will be recalculated on the basis of three contacting pairs (step 3). These calculation methods can handle both the involute and nonvolute gear actions, HCR gearing, etc.

The individual gear-tooth pair stiffness can be expressed as

$$\mathrm{KP}(k)_i = \frac{Q(k)_i}{\delta(k)_i} \tag{7}$$

If the effective errors prevent contact, $\mathrm{KP}(k)_i = 0$. The sum of gear-tooth pair stiffnesses for all pairs in contact at position i represents the variable mesh stiffness (KG),

$$\mathrm{KG}_i = \sum_{1}^{K} KP(k)_i \tag{8}$$

The load carried by each of the pairs moving through the mesh arc in the static mode can be determined as

$$\mathrm{Q}(k)_i = \frac{\mathrm{KP}(k)_i}{\mathrm{KG}_i}(Q_t) \tag{9}$$

where Q_t is the total normal static load carried by the gears at any mesh position i in the static mode. For any mesh arc position i, the calculated K^{th} gear-tooth pair stiffness $\mathrm{KP}(k)_i$, mesh stiffness KG, and load sharing incorporate the effects due to manufactured profile errors, profile modifications, and deflections by means of the iterated numerical solutions of equations (3) to (9).

Deflections and profile faults will cause gears to contact away from the theoretical line of action.

For the instances when the contact points are not on the theoretical lines of action (nonconjugate action), we must refer to instantaneous pressure angles, instantaneous lines of action, and transmission ratios. The need for instantaneous lines of action was indicated in references 11 and 12. Figure 6 is used to define the instantaneous parameters (designated by ′) for the contact point A′ (defined by UCP(k), VCP(k) in the U, V coordinate system). For example, the distance to the instantaneous pitch point PP′ is

$$\mathrm{PPD}' = \frac{\mathrm{RBC1}}{\cos \alpha'} \tag{10}$$

where α' is the instantaneous pressure angle

$$\alpha' = \alpha_{\mathrm{A1}} + \alpha_{\mathrm{B1}} \tag{11}$$

where

$\alpha_{\mathrm{A1}} = \arcsin\ (\mathrm{UCP}(k)/\mathrm{RCP1})$
$\alpha_{\mathrm{B1}} = \arctan\ (\mathrm{RCCP1}/\mathrm{RBC1})$

Again, using figure 6, the instantaneous transmission ratio is

$$\mathrm{TR}' = \frac{\mathrm{C} - \mathrm{PPD}'}{\mathrm{PPD}'} \tag{12}$$

The involute (theoretical) transmission ratio is

$$\mathrm{TR} = \frac{\mathrm{RPC2}}{\mathit{RPC1}} \tag{13}$$

The instantaneous base circle (gear 2) is

$$\mathrm{RBC2}' = \mathrm{RBC1} \times \mathrm{TR}' \tag{14}$$

The equivalent instantaneous radius of curvature (gear 1) is

$$RCCP1' = \sqrt{(RCP1)^2 - (RBC1)^2} \tag{15}$$

And the equivalent instantaneous radius of curvature (gear 2) is

$$RCCP2' = \sqrt{(RCP2)^2 - (RBC2')^2} \tag{16}$$

The same procedure is used for determining the instantaneous parameters as the above gear pair k traverses the mesh arc and, similarly, for other gear pairs. The instantaneous transmission ratio TR′ is influenced by the deformations in the contact zone and tooth profile errors. It is important to note that for no-load and no-surface fault conditions TR′ = TR, and similar analogy exists for other parameters.

Discussion of Gear Mesh Parameters

The performed analyses have indicated that the gear-hub flexibility can have a significant effect on the operational gear-mesh stiffness, KG. The hub stiffness factor (HSF) will be used to indicate a degree of influence of the hub flexibility on the overall gear-mesh stiffness.

$$HSF = \frac{KG_{max}}{KG^*_{max}} \tag{17}$$

where

KG_{max} maximum attainable gear mesh stiffness with designated hubs

KG^*_{max} maximum gear-mesh stiffness with torsionally rigid max hubs, circumferential fixity at the gear root circle

The torsionally rigid hubs can be theoretically obtained when the radius of circumferential or torsional fixity will coincide with the root circle. The opposite case can be visualized with the thin hubs being fixed to small shafts. A combination of rigid hubs for both gears is identified by HSF = 1.0.

Tables 1 and 2 indicate substantial changes in the contact ratio with increasing loads and/or gear-hub flexibilities. By increasing the hub torsional flexibility (lower HSF), the contact ratio increases, the variation of the instantaneous transmission ratio (TR′) increases, and the sensitivity to gear-tooth errors decreases. The opposite occurs by decreasing the hub flexibility. The gear-tooth contacts due to deflections and errors may occur off the theoretical line of action, thus affecting the transmission ratio. The ΔTR can be viewed as a percent change in the output torque. The approximate variation (cycling) of TR′ is illustrated in figure 7. The maximum variation in TR′ is defined as ΔTR′.

Various profile errors, pitting, and the previously discussed hub flexibility can affect the mesh stiffness characteristics to varying degrees. A case where only one of the meshing gears has surface

TABLE 1. - EFFECTS OF GEAR FLEXIBILITY ON MESH STIFFNESS, TRANSMISSION RATIO, AND CONTACT RATIO

[All gears without errors or modifications $RH1_f$, $RH2_f$ = torsional fixity radius; gears 1, 2.]

$RH1_f$, mm	$RH2_f$, mm	KG_{max}, N/m	KG_f, N/mm^2	HSF	ΔTR, percent	CR
10.0	14.5	3.07×10^8	1.21×10^4	0.476	2.4	2.47
12.7	18.3	3.80	1.50	.591	1.9	2.42
12.7	38.1	5.08	2.00	.794	1.6	2.36
38.1	114.3	6.36	2.50	.992	1.0	2.32
47.2	148.8	6.45	2.54	1.0	1.0	2.32

TABLE 2. - LOAD EFFECTS ON TRANSMISSION RATIO AND CONTACT RATIO GEARS
[32 and 96T; 8DP; 14.5° PA; CR_T = 2.14; HSF = 0.992.]

Load, N/mm	TR, percent	CR
88	0.8	2.29
175	1.0	2.32
350	1.0	2.38
525	1.8	2.43
700	2.2	2.45

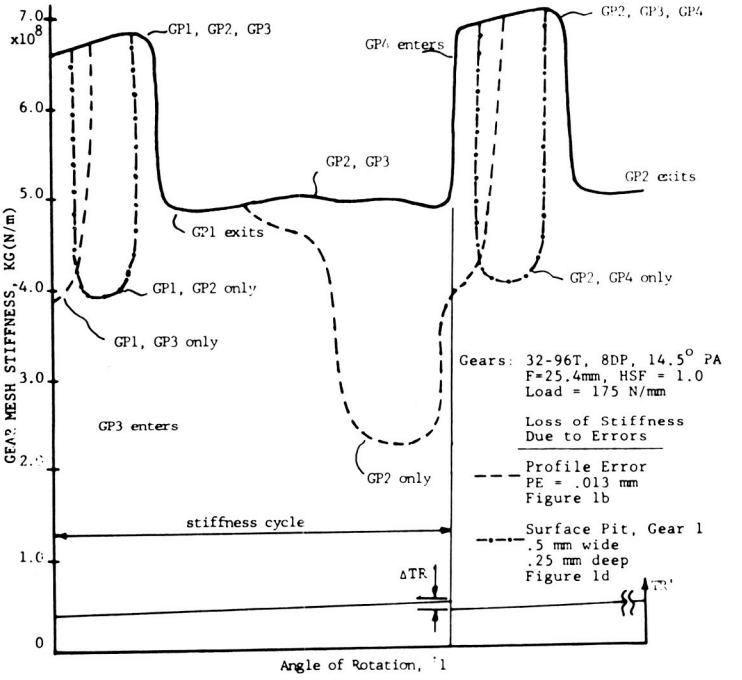

Figure 7. - Effects of profile faults on gear mesh stiffness.

imperfections will be considered first. For example, with torsionally flexible hubs (HSF = 0.5), the sinusoidal errors of 0.013 mm (0.0005 in.) and narrow surface pits 0.5 mm wide (0.02 in.) were absorbed by the mesh flexibility consequently producing the errorless mesh stiffness characteristics. On the other hand, when the hubs were torsionally rigid (HSF = 1) the mesh flexibility was not able to absorb the errors of above magnitudes. Unabsorbed errors can cause loss of stiffness thus causing significant changes in the gear-mesh stiffness characteristics (dashed lines in fig. 7). With increasing hub flexibility there was a gradual return to normal mesh stiffness characteristics, that is, the flexibilities in the mesh were able to narrow or bridge the noncontact zones. For example, a 32- and 96-tooth gear pair mesh with HSF = 0.6 was able to absorb a portion of the sinusoidal error by eliminating about 50 percent of the mesh stiffness interruption shown in figure 7. Unabsorbed errors in the NCR gearing will cause a complete momentary loss of gear mesh stiffness.

The developed method can also be used to investigate other error combinations acting on both gears. For example, errors shown in figure 1(b) with PE1 and PE2 of 0.013 mm are nearly self-compensating in terms of developed stiffness characteristics. Other profile combinations, especially of large error magnitudes, could lead theoretically to nonoperational contact ratios or to unacceptable interruptions of the mesh stiffness function. The sinusoidal profile errors of approximately one cycle (fig. 1(b)) and 0.013 mm in magnitude are probably the maximum tolerable profile errors in accurate spur gearing applications.

It can be also noted that by selecting an appropriate combination of transmitted loads and gear-

hub flexibilities some of the NCR gear pairs can be theoretically made to operate in the HCR regime.

Dynamic Model

The gear train shown in figure 8 was used in dynamic simulations. This model is assumed to represent one of the practical cases in gearing. The dynamic model is based on the same coordinates as the static model. The developed gear-mesh stiffness characteristics and other parameters were then automatically transferred to the dynamic simulation of the system.

The equations of motion for this model along the instantaneous (noninvolute) line of action can be given in the following form:

$$J_D\ddot{\psi}_D + C_{B1}\dot{\psi}_D + C_{DS}(\dot{\psi}_D - \dot{\psi}_1) + K_{DS}(\psi_D - \psi_1) = T_{IN} \tag{18}$$

$$J_{G1}\ddot{\psi}_1 + C_{B2}\dot{\psi}_1 + C_{DS}(\dot{\psi}_1 - \dot{\psi}_D) + K_{DS}(\psi_1 - \psi_D) + CG_i(\mathrm{RBC1}\dot{\psi}_1 - \mathrm{RBC2'}\dot{\psi}_2)\mathrm{RBC1}$$
$$+ \mathrm{KG}_i(\mathrm{RBC1}\psi_1 - \mathrm{RBC2'}\psi_n)\mathrm{RBC1} = 0 \tag{19}$$

$$J_{G2}\ddot{\psi}_2 + C_{B3}\dot{\psi}_2 + C_{LS}(\dot{\psi}_2 - \dot{\psi}_L) + K_{LS}(\psi_2 - \psi_L) + CG_i(\mathrm{RBC2'}\dot{\psi}_2 - \mathrm{RBC1}\dot{\psi}_1)\mathrm{RBC2'}$$
$$+ \mathrm{KG}_i(\mathrm{RBC2'}\psi_2 - \mathrm{RBC1}\psi_1)\mathrm{RBC2'} = 0 \tag{20}$$

$$J_L\ddot{\psi}_L + C_{B4}\dot{\psi}_L + C_{LS}(\dot{\psi}_L - \dot{\psi}_2) + K_{LS}(\psi_L - \psi_2) = -T_{IN} \times TR' = -T_L(TR') \tag{21}$$

In equations (19) and (20) KG_i represents the variable gear pair mesh stiffness and is a function of gear-tooth profile errors and modifications, deflections of gear teeth, load sharing, and height of engagement for any angular position i of engagement. The mesh stiffness cycle is also illustrated in figure 7. The basic sources of excitation for a rotating pair of gears are the variation and interruptions of mesh stiffness and the changes in the transmission ratio caused by noninvolute action. The input torque T_{IN} is assumed to be constant while the output of load torque T_L is a function of the instantaneous transmission ratio shown as the T_L(TR'). In this study it is assumed that the instantaneous transmission ratio is dominated by the incoming tooth pair as it moves through one gear-mesh stiffness cycle.

Operational situations, which may involve momentary disengagement of gears in mesh, will impose the following conditions on the dynamic gear-mesh forces in equations (3) and (4); if $\mathrm{RBC2'}\psi_2 < \mathrm{RBC1}\psi_1$, then

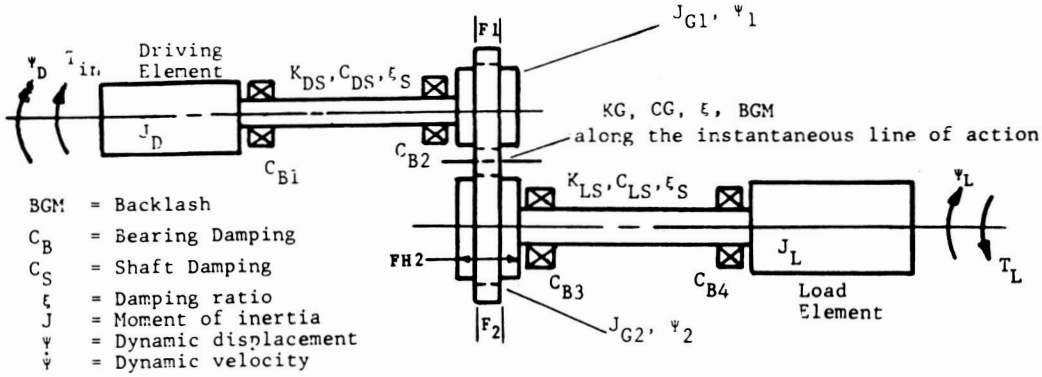

Figure 8. - Gear train dynamics model.

$$(QD_t)_i = CG_i(RBC1\dot{\psi}_1 - RBC2'\dot{\psi}) + KG_i(RBC1\psi_1 - RBC2'\psi_2) \tag{22}$$

if $RBC2'\psi_2 > RBC1\psi_1$ and $(RBC2'\psi_2 - RBC1\psi_2) < BGM$, then

$$(QD_t)_i = 0 \tag{23}$$

if $RBC2'\psi_2 > RBC1\psi_1$ and $(RBC2'\psi_2 - RBC1\psi_1) > BGM$, then

$$(QD_t)_i = CG_i(RBC1\psi_1 - RBC2'\psi_2) + KG_i(RBC1\dot{\psi}_1 - RBC2'\dot{\psi}_2) - BGM) \tag{24}$$

Also, when $KG_i = 0$, $(QD_t)_i = 0$.

The equivalent damping in gear mesh CG_i was related to KG_i by means of a critical damping coefficient ξ.

A fourth-order Runge-Kutta integration scheme was used to integrate the indicated differential equations of motion. The initial displacements $\psi_1(0)$, $\psi_2(0)$, $\psi_D(0)$, and $\psi_L(0)$ were determined by statically twisting the entire system with the prescribed T_{IN} and T_L torques. For the initial velocities $\dot{\psi}_1(0)$, $\dot{\psi}_2(0)$, $\dot{\psi}_D(0)$, and $\dot{\psi}_L(0)$, the anticipated steady-state involute action velocities were selected.

The numerical integration of the equations of motion (eqs. (18) to (21)) is carried out for a length of time equivalent to the time required for the startup transient to decay. This time is assumed to be equal to five times the longest system natural period. The integration time step was taken either as one tenth of the shortest system natural period or 1 percent of the mesh stiffness period with $CR < 2$ (2 percent for $CR > 2$), whichever is smaller.

For illustration purposes two computer outputs for the static and dynamic loads are shown in figures 9 and 10. The static and dynamic load distributions are shown along the gear-tooth profiles as the gear tooth traverses the meshing arc. The dynamic load can be also plotted as a function of time.

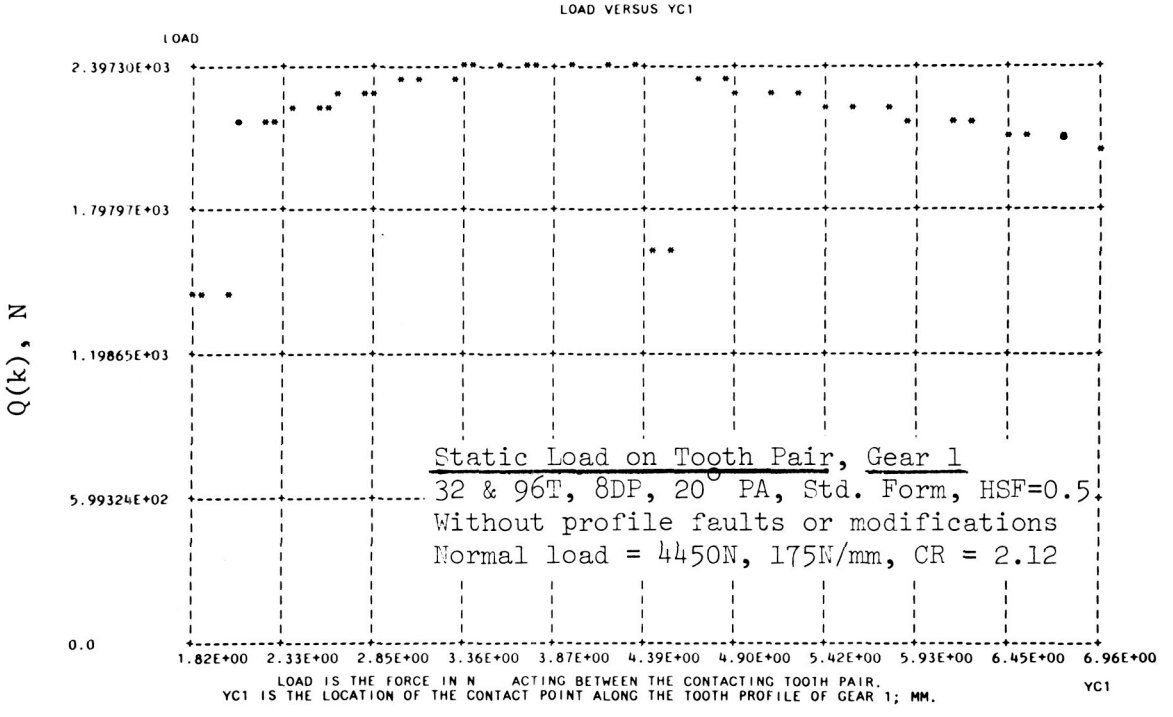

Figure 9. - Typical static load distribution.

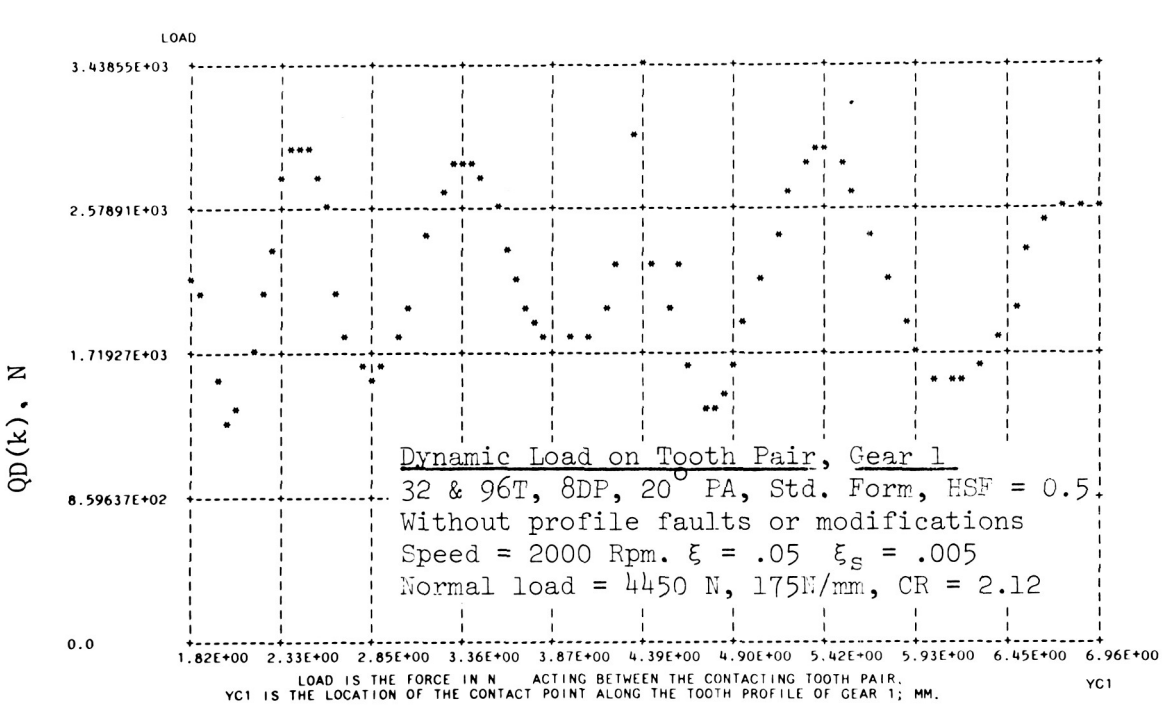

Figure 10. - Typical dynamic load distribution.

The dynamic load QD(k) for a contacting gear-tooth pair k in the mesh position i was established as

$$QD(k)_i = \frac{KP(k)_i}{KG_i}(QD_t)_i \tag{25}$$

In this study the dynamic load factors were defined as

$$(DF_1)_i = \frac{(QD_t)_i}{Q_t} \tag{26}$$

and

$$(DF_2)_i = \frac{QD(k)_i}{Q(k)_i} \tag{27}$$

where DF_1 can be interpreted as the dynamic load factor for the mesh or as the dynamic load factor for the gear pair, adjacent shafts, and bearings and where DF_2 is the dynamic load factor for an individual gear-tooth pair traversing the mesh arc. The DF_2 is of main significance when the strength of the gear teeth is of primary importance. The larger of the two dynamic load factors will be defined as the dynamic load factor for design, DF.

Dynamic Analysis

The dynamic loads are influenced by a large number of variables such as the mass moments of inertia of all elements, shaft stiffnesses, transmitted loads, gear-mesh stiffness characteristics, damping in the system, amount of backlash and speed. The mesh stiffness characteristics are affected

by various error-caused interruptions. Figure 7 suggests considerable variations of the harmonic contents. Consequently, the harmonic contents of the mesh stiffness characteristics can excite a number of natural frequencies.

Because of the large number of variables, only four sets of HCR and NCR gearing (table 3) loaded with a normal load of 4450 N or 175 N/mm (1000 lb/in) will be discussed.

The developed method has the capability for analyzing the distribution of the dynamic loads, dynamic factors, load sharing, contact-Hertz stress (P_H), and the contact stress-sliding velocity product (PV) for the entire meshing zone.

Figure 11 illustrates the dynamic characteristics in terms of (DF) for a gear drive (fig. 8) with errorless HCR gearsets. The trends indicate that various gear drive systems could be designated for best performance in terms of acceptable dynamic loads by proper selection of masses, gears, gear-mesh and shafting flexibilities, and damping. The primary excitation for errorless gears with $CR \neq 2.0$ is the inherent variation in mesh stiffness. An interestingly new response characteristic is exhibited by several gearsets having $CR = 2.0$ (almost flat gear-mesh stiffness). The main excitation for $CR = 2.0$ is due to variation in the transmission ratio (ΔTR) caused by noninvolute action. However, $CR = 2.0$ could be obtained only for some specific load and geometrical conditions.

The HCR gearing with $CR = 2.0$ showed reasonably good tolerance to several types of surface faults. In general, the dynamic loads can be reduced by introducing higher damping, higher applied loads, and lower HSF's.

TABLE 3 NCR and HCR Gearing Grouping

1. Inherent HCR gearing with small pressure angle and fine pitch represented by 32 & 96T, 8DP, 14.5° PA, CR_T = 2.14.

2. Long addendum HCR gearing represented by:
   32 and 96T, 8DP, 20° PA, 1.1 x std. addendum, CR_T = 2.15, CR = 2.42, HSF = 0.5, and HSF = 1.0
   32 & 96T, 8DP, 25° PA, 1.1 x std. addendum, CR_T = 1.89, CR = 2.16, HSF=.5

3. HCR gearing with CR = 2.0 represented by a number of 20° PA gear sets, HSF, and loads. For example, 32 & 96T, 8DP, 20° PA, CR_T = 1.76, CR = 2.0, HSF = .73

4. NCR gearing represented by:
   20 & 20T, 4DP, 20° PA, CR_T = 1.56; CR = 1.67, HSF = .7
   32 & 96T, 8DP, 25° PA, CR_T = 1.53; CR = 1.72, HSF = 1.0
   40 & 40T, 8DP, 20° PA, CR_T = 1.51, CR = 1.68, HSF = 1.0

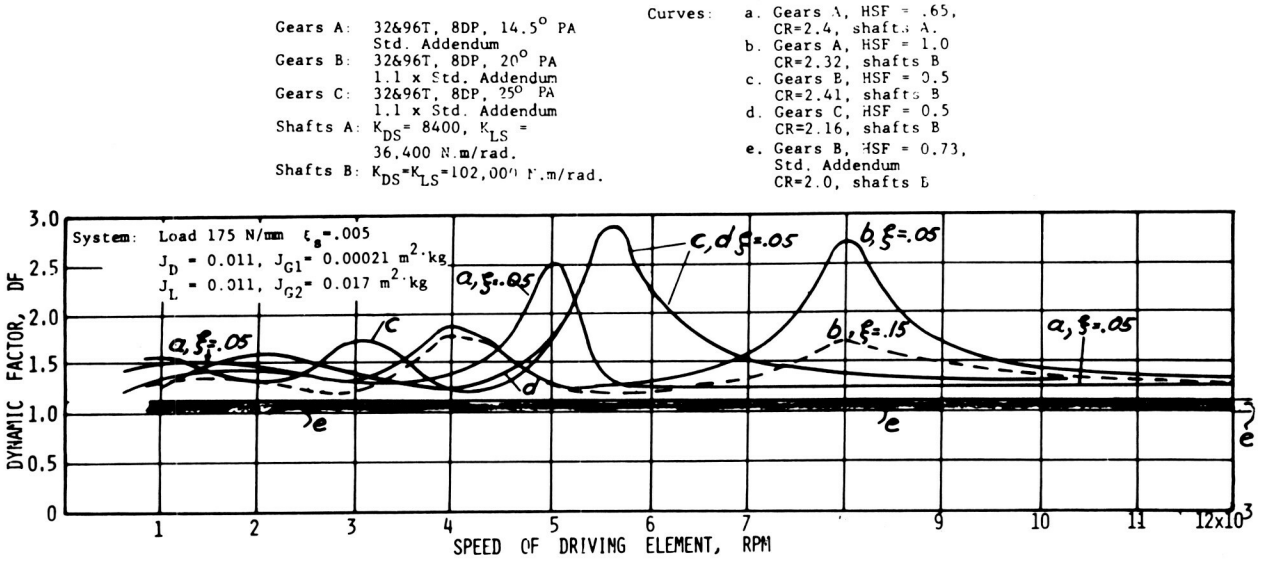

Figure 11. - Damping and system flexibility effects on dynamic factors for errorless HCR gear sets.

Reference 17 indicated a 300 percent increase in dynamic amplitudes caused by a zero stiffness zone due to a single tooth pit. In this study surface imperfections were assigned to all teeth for a given gear.

The analyses tend to suggest that the main sources of excitation are the variable mesh stiffness function and its interruptions.

The effects of unabsorbed profile surface imperfections (sinusoidal and pitting) are illustrated in figures 12 and 13 for the HCR and NCR gearing. In the presented cases momentary gear separation can occur when DF>2. The resonant peaks are the average dynamic load factors based on the backlash between zero and 0.25 mm.

The unabsorbed errors in the NCR situations considered caused a momentary loss of mesh

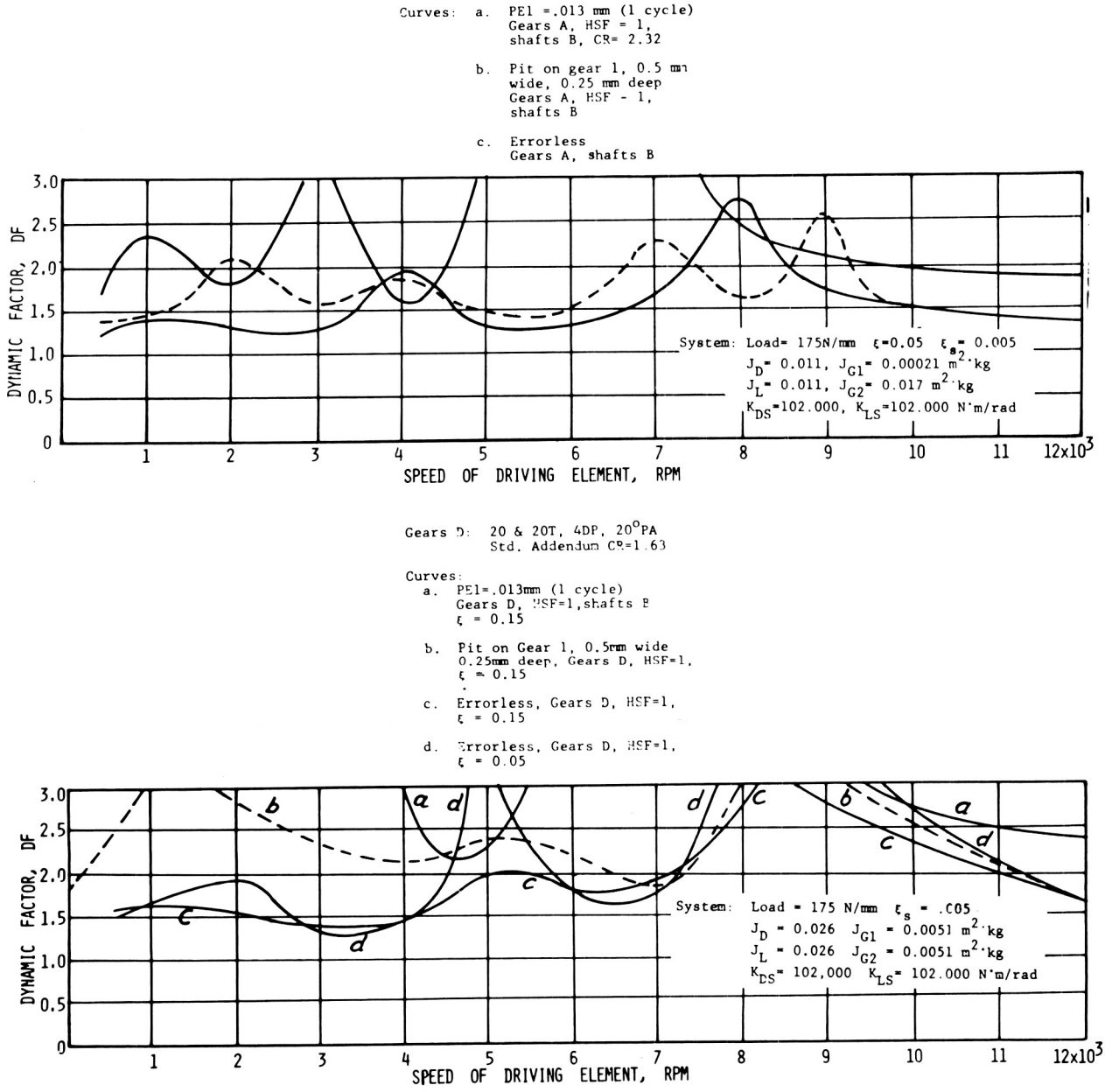

Figure 13. - Influence of profile faults on dynamic factors for a characteristic NCR gear pair.

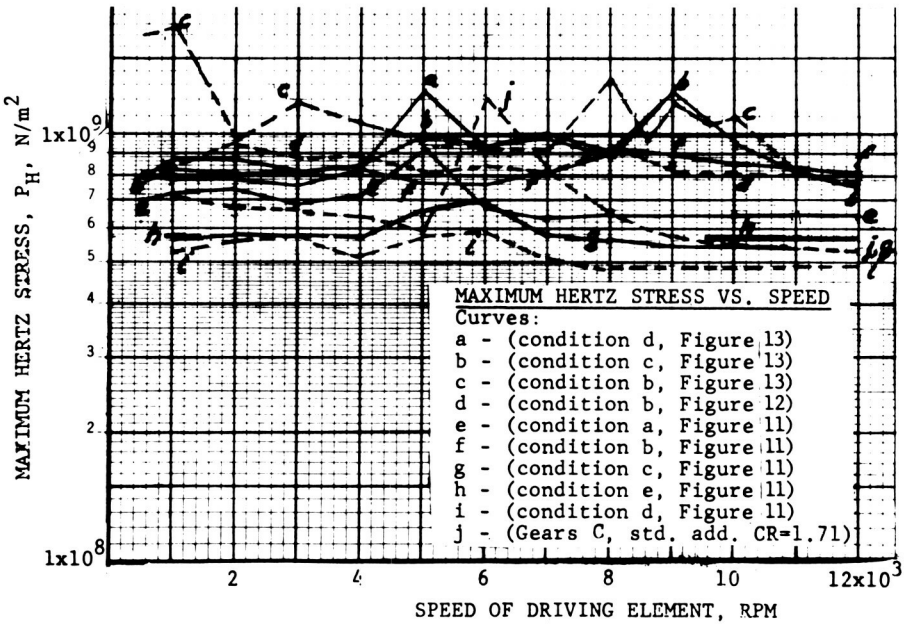

Figure 14. - Maximum Hertz stress.

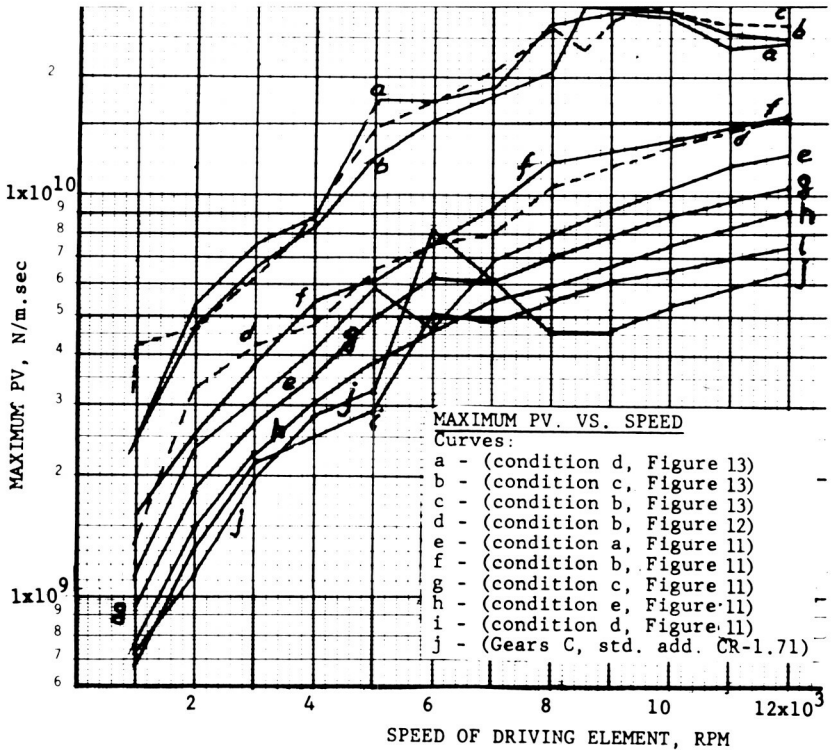

Figure 15. - Maximum product of Hertz stress and sliding velocity.

stiffness, resulting in high dynamic loads and gear separation over a wide region of considered speeds. In the slow speed range there is a large zone of high dynamic load factors affected by a number of the mesh stiffness function harmonics and separation of gears. The same unabsorbed errors in the HCR gearing cause only a partial loss of stiffness and, thus, indicate lower error-caused dynamic loads than in the NCR gearing. The ΔTR quantity which represents variation of load torque due to noninvolute action appears to be of secondary importance as a source of excitation.

References

1. Buckingham, E.: Dynamic Loads on Gear Teeth. Report of Special Research Committee on the Strength of Gear Teeth, ASME, New York, 1931.
2. Tuplin, W. A.: Dynamic Loads on Gear Teeth. Machine Design, vol. 25, Oct. 1953, pp. 203-211.
3. Reswick, J. B.: Dynamic Loads on Spur and Helical Gear Teeth. ASME, vol. 77, no. 5, July 1955, pp. 635-644.
4. Nakada, T., and Utagawa, M.: Dynamic Loads Caused by the Varying Elasticity of Mating Gear Teeth. Proc. 6th Japan National Congress on Applied Mechanics, 1956, pp. 493-497.
5. Zeman, J.: Dynamische Zusatzkraefte in Zahnradgetrieben. Z. Ver. Dtsch. Ing., vol. 99, 1957, pp. 244-254.
6. Harris, S. L.: Dynamic Loads on the Teeth of Spur Gears. Proc. Institute of Mechanical Engineers, vol. 172, 1958, pp. 87-112.
7. Richardson, H. H.: Static and Dynamic Load, Stress and Deflection Cycles in Spur Gearing. Sc.D. Thesis, Department of Mechanical Engineering, M.I.T., Cambridge, Mass., 1958.
8. Bohm, F.: Drehschwingungen von Zahnradgetrieben. Oesterr. Ing., vol. 13, no. 2, 1959, pp. 82-103.
9. Staph, H. E.: A Parametric Analysis of High-Contact-Ratio Spur Gears. ASLE Trans., vol. 19, no. 3, 1976, pp. 201-215.
10. Cornell, R. W.; and Westervelt; W. W.: Dynamic Tooth Loads and Stressing for High Contact Ratio Spur Gears, ASME Paper 77-DET-101.
11. Kasuba, R.; and Evans, J. W.: An Extended Model for Determining Dynamic Loads in Spur Gearing. J. Eng. Ind., vol. 103, no. 3, April 1981, pp. 398-409.
12. Niemann, G.; and Baethge, J.: Drehwegfehler, Zahnfederharte und Gerausch bei Stirnradern, Z. Ver. Dtsch. Ing., vol. 112, no. 4, 1970, pp. 205-214.
13. Weber, C.: The Deformation of Loaded Gears and the Effect on Their Load-Carrying Capacity. Part I, Department of Scientific and Industrial Research, Sponsored Research (Germany) no. 3, London, 1949.
14. Attia, A. Y.: Deflection of Spur Gear Teeth Cut in Thin Rims, J. Eng. Ind., vol. 86, no. 4, Nov. 1964, pp. 33-342.
15. Chakraborty, J.; and Hunashikati, H. G.: Determination of the Combined Mesh Stiffness of a Spur Gear Pair Under Load. ASME Paper 74-DET-39, 1974.
16. Utagawa, M.; and Harada, T.: Dynamic Loads on Spur Gear Teeth Having Pitch Errors at High Speed. Bull. JSME, vol. 5, no. 18, 1962, pp. 374-381.
17. Drosjack, M. J.; and Houser, D. R.: An Experimental and Theoretical Study of the Effects of Simulated Pitch Line Pitting on the Vibration of a Geared System. ASME Paper 77-DET-123.